

Symmetry-enforced ideal lantern-like phonons in ternary nitride Li_6WN_4

Xiaotian Wang,^{1,*} Feng Zhou,^{1,*} Tie Yang,¹ Minquan Kuang,¹ Zhi-Ming Yu,^{2,†} and Gang Zhang^{3,‡}

¹*School of Physical Science and Technology, Southwest University, Chongqing 400715, China.*

²*Key Lab of Advanced Optoelectronic Quantum Architecture and Measurement (MOE),
Beijing Key Lab of Nanophotonics & Ultrafine Optoelectronic Systems,
and School of Physics, Beijing Institute of Technology, Beijing 100081, China.*

³*Institute of High Performance Computing, Agency for Science,
Technology and Research (A*STAR), 138632, Singapore.*

Condensed matter systems contain both fermionic and bosonic quasiparticles. Owing to the constraint imposed by the Fermi level, ideal material candidate for the emergent particles with higher-dimensional degeneracy manifold (i.e., nodal lines and nodal surfaces) has not been found in electronic systems. This paper demonstrates that according to the first-principle calculations and symmetry analysis, realistic ternary nitride Li_6WN_4 features ideal (nearly flat) nodal-surface and nodal-line structures in its phonon spectra. These nodal degeneracies are shaped like lanterns, and their existence is guaranteed by nonsymmorphic symmetry. The corresponding topological phonon surface state covers exactly half the surface Brillouin zone (BZ) and can thereby be distinguished from those of conventional nodal-line and nodal-surface semimetals. The results of our study demonstrate the existence of ideal lantern-like phonons in realistic materials, which enriches the classification of topological quantum phases and provides a good basis for investigating the interaction between nodal-line and nodal-surface phonons in a single material.

Condensed matter systems [1, 2] contain both fermionic and bosonic quasiparticles. The existence of the former in electronic structures [3–9] has been widely predicted and verified; by contrast, the existence of topological bosonic excitations [10–14] has been rarely reported. According to the dimension of the degeneracy manifold, topological semimetals can be classified into nodal-point [15–21], nodal-line [22–26], and nodal-surface semimetals [27–29]. Both nodal-line and nodal-surface semimetals exhibit many intriguing phenomena [29, 31–33]. For example, it has been predicted that the nodal lines have drumhead-like surface states that cover a finite region in the surface Brillouin zone (BZ) or torus surface states spanning over the entire BZ. Although the nodal surface cannot have an intrinsic Chern number, it can have an induced one [34], which can be any integer value, depending on the chiral particles in the BZ. To determine the properties of nodal lines or nodal surfaces, the line or surface should preferably have a relatively flat energy dispersion. In addition, in electronic systems, the line or surface should be close to the Fermi level. Therefore, ideal nodal semimetals (in particular, ideal nodal-surface semimetals) are still missing in electronic systems.

Phonons, which are the basic emergent kind of bosons in crystalline lattices, can also display nontrivial degeneracy in their spectra. Because the Pauli exclusion principle does not apply to phonons, it provides a feasible basis for investigating bosonic excitations in a wide frequency range without the rigorous constraint of the fermion level. Researchers are currently searching for ideal topological phases in phonon systems [10, 14, 35–46]. In particu-

lar, the existence of Weyl, Dirac, triple point, nodal line phonons in the phonon spectra of several materials has been predicted, and the existence in some of them has been experimentally confirmed [39, 46]. However, the existence of nodal-surface phonons has not been reported.

A natural question is whether ideal nodal-surface phonons can exist in realistic materials. In this paper, we answer this question affirmatively. *For the first time*, based on first-principle calculations and symmetry analysis, we predict the existence of nodal-surface phonons in ternary nitridotungstate Li_6WN_4 , which has been experimentally synthesized [47] via the solid state reaction of lithium subnitride (Li_3N) with W in a nitrogen atmosphere. The Li_6WN_4 material has two nodal surfaces in the $k_x = \pi$ and $k_y = \pi$ planes, respectively, the existence of which is guaranteed by nonsymmorphic screw-rotational symmetry and time-reversal symmetry. Remarkably, the two nodal surfaces are ideal in that (i) the two bands forming the nodal surfaces are well separated from other bands and in that (ii) the nodal surface is approximately flat in energy, with energy variations of less than 0.25 THz (approximately 1.00 meV). These characteristics have not been observed for other proposed nodal surface materials. Moreover, the two bands that form the nodal surfaces become degenerate in the Z-A path of the $k_z = \pi$ planes, thereby leading to two symmetry-enforced nodal lines. Eventually, the two nodal surfaces and two nodal lines in Li_6WN_4 result in exotic nodal-lantern phonon excitations, as illustrated in Fig. 2(c) and Fig. S1. Hence, this work presents novel topological phases of phonon systems, predicts ideal material candidate, and paves the way for investigating nodal-lantern phonons in experiments.

The density-functional theory [48] was used to calculate the ground state of this material, and the GGA-PBE formalism [49] was used for the exchange-correlation

* These authors have contributed equally to this work.

† zhiming_yu@bit.edu.cn

‡ zhangg@ihpc.a-star.edu.sg

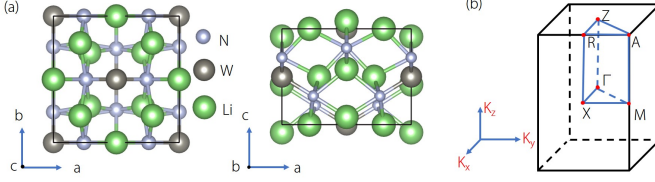


FIG. 1. Crystal structure of Li_6WN_4 material with P42/nmc type structure under different viewsides. (b) Bulk BZ and high-symmetry points.

functional. In addition, the projector augmented-wave method was used for the interactions between ions and valence electrons, and the energy cutoff was set to 600 eV. A Γ -centered k -mesh of $5 \times 5 \times 6$ size was used to sample the BZ. Moreover, lattice dynamic calculations were performed to obtain the phonon dispersion of Li_6WN_4 at equilibrium lattice constants in the PHONOPY package [50] with density-functional perturbation theory. The topological characteristics of the [001] phonon surface states were calculated by constructing a Wannier tight-binding Hamiltonian for phonons [51].

As shown in Fig. 1a, Li_6WN_4 is a tetragonal material with space group (SG) No. 137 (P42/nmc). The atomic positions are as follows: W is located at the 2a (0.25, 0.75, 0.25), N at the 8g (0.25, 0.995, 0.05), Li (1) at the 4d (0.25, 0.25, 0.338), and Li (2) at the 8f (0.537, 0.463, 0.25) Wyckoff positions. The crystal structure of Li_6WN_4 is completely relaxed according to the first-principle calculations; the computed lattice constants $a = b = 6.71 \text{ \AA}$ and $c = 4.94 \text{ \AA}$ agree well with the experimental results ($a = b = 6.675 \text{ \AA}$ and $c = 4.928 \text{ \AA}$).

The symmetry operators of Li_6WN_4 are generated via fourfold screw rotation $S_{4z} = \{C_{4z} | 00 \frac{1}{2}\}$, twofold screw rotation $S_{2x} = \{C_{2x} | \frac{1}{2} \frac{1}{2} 0\}$, spatial inversion $\{I | \frac{1}{2} \frac{1}{2} 0\}$, and time-reversal symmetry \mathcal{T} . Hence, Li_6WN_4 has three mirror symmetries: M_x , M_y , and M_z . Because we are interested in the phonon spectrum of Li_6WN_4 , the spin-orbit coupling effect is neglected, indicating that the 2π rotation equals 1 and $\mathcal{T}^2 = 1$.

In this work, the topological signature of the phonon dispersion of Li_6WN_4 was studied. The calculated phonon band along the high-symmetry paths (see Fig. 1b) is shown in Fig. 2a. The absence of imaginary frequency modes in the phonon dispersion indicates that Li_6WN_4 is dynamically stable. We focused on the two phonon bands appearing in the 22.5-24.5 THz range; they are well separated from other energy bands. Evidently, the two phonon bands become twofold degenerate along the X-M-A-R-X and Z-A paths. For clarity, we divided the doubly degenerate phonon bands in the 22.5-24.5 THz range into the two regions R2 and R3, as shown in Fig. 2b. The degeneracies in the R2 and R3 regions are discussed separately.

First, the double degeneracies along the X-M-A-R-X path were studied (R2 in Fig. 2b). All these high-symmetry paths lie in the BZ boundary, e.g., in the $k_x =$

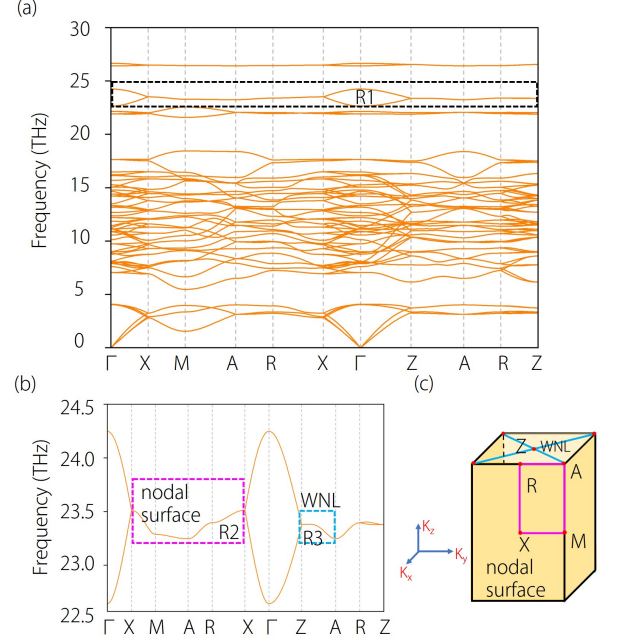


FIG. 2. (a) Phonon dispersion of Li_6WN_4 along Γ -X-M-A-R-X- Γ -Z-A-R-Z paths; (b) enlarged frequencies of Li_6WN_4 with nodal surface phonons (see R2) and Weyl nodal line (WNL)-phonons (See R3); (c) Schematic diagram of nodal phonon states of R2 and R3 in 3D BZ.

π plane (see Fig. 2c). In Fig. 3a and b, we divided the A-X paths into 5 parts and selected some other symmetry points along the A-X path: b1, b2, b3, and b4. The phonon dispersion along the a1-b1-a1', a2-b2-a2', a3-b3-a3', and a4-b4-a4' paths are shown in Fig. 3c and Fig. S2, respectively. Evidently, two non-degenerate phonon bands linearly cross at b1, b2, b3, and b4.

In fact, the two phonon bands become degenerate in the entire $k_x = \pi$ plane (see the schematic diagram in Fig. 3a), which leads to the creation of a nodal surface. The nodal surface is guaranteed by nonsymmorphic S_{2x} symmetry and \mathcal{T} symmetry because any generic point in the $k_x = \pi$ plane is invariant under $\mathcal{T}S_{2x}$ symmetry and $(\mathcal{T}S_{2x})^2 = -1$ in the $k_x = \pi$ plane. Owing to the fourfold screw rotation S_{4z} , there must exist another nodal surface in the $k_y = \pi$ plane. It should be noted that while the z-direction represents a screw rotation axis, there is no nodal surface in the $k_z = \pi$ plane, which can be directly inferred from the phonon dispersion along the R-Z path. This is because S_{4z}^2 is equivalent to a symmorphic operator and $(\mathcal{T}S_{4z}^2)^2 = 1$ in the $k_z = \pi$ plane. However, although the existence of two nodal surfaces in the $k_x = \pi$ and $k_y = \pi$ planes is guaranteed owing to the symmetry characteristics, the energy dispersion of the surface is not constrained by these symmetries.

To the best of our knowledge, the existence of an ideal topological nodal-surface semimetal with a flat nodal surface state has not been reported [27]. Fortunately, the nodal-surface phonons in Li_6WN_4 are very flat in energy

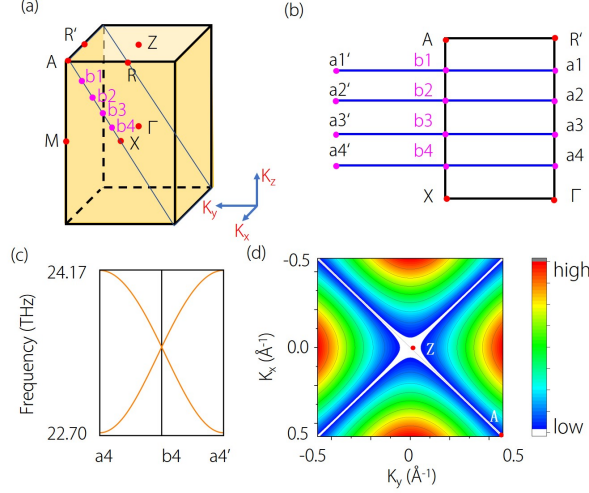


FIG. 3. (a) Schematic diagram of nodal surface states in $k_x=\pi$ and $k_y=\pi$ planes; (b) some symmetry points of [011] plane; a1, a2, a3, and a4 and b1, b2, b3, and b4 are located at equal distances between R' (A) and Γ (X); (c) phonon dispersion along a4-b4-a4' paths; (d) shape of one pair of Z-centered WNLs in $k_z=\pi$ plane.

with energy variations of less than 0.25 THz (approximately 1.00 meV). More importantly, the phonon band structure is “clean” in the sense that the bands forming the surface are well separated from the other bands. Another feature of the nodal-surface phonon is that it exhibits linear dispersion along the direction normal to the surface; in addition, the linear energy range is considerable large for most points on the surface, as indicated in Fig. 2b. To present these characteristics more clearly, the calculated energy dispersion for points on the surface along the transverse direction is presented in Fig. 3c and Fig. S2c, showing the linear energy range for the path away from the surface is considerable large.

In the next step, the degeneracies along the Z-A path are discussed (see R3 in Fig. 2b). This is an essential nodal line protected by M_z symmetry and twofold rotation along the (110) direction. The low-energy effective Hamiltonian expanding around a generic point on the Z-A path can be written as follows [52]:

$$\mathcal{H} = c_1 + c_2\sigma_3(k_x - k_y) + c_3\sigma_1k_z, \quad (1)$$

where σ_i ($i = 1, 2, 3$) is the Pauli matrix, and the model parameter c_i depends on the material and $k_{x(y)}$; the momentum is measured from the generic point on the Z-A path. To examine the nontrivial topological behavior of this nodal line, we calculate the Berry phase for a closed loop surrounding the line, expressed as:

$$P_B = \oint_c \mathbf{A}(\mathbf{k}) \cdot d\mathbf{k} \quad (2)$$

with $\mathbf{A}(\mathbf{k}) = -i \langle \varphi(\mathbf{k}) | \nabla_{\mathbf{k}} | \varphi(\mathbf{k}) \rangle$ the Berry connection and $\varphi(\mathbf{k})$ the periodic part of the Bloch function. According to our results, we obtain $P_B = \pi$. Then one

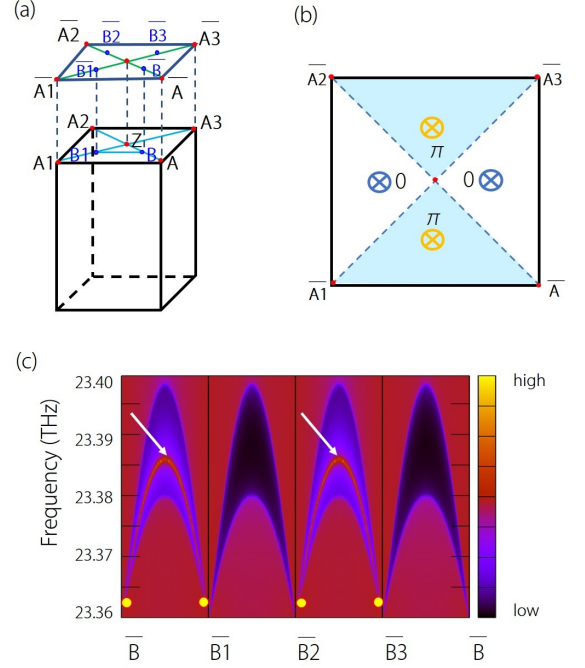


FIG. 4. (a) projection of WNL onto [001] surface and some surface symmetry points $\bar{A}, \bar{A}_1, \bar{A}_2, \bar{A}_3, \bar{B}, \bar{B}_1, \bar{B}_2, \bar{B}_3$ of [001] surface; (b) schematic diagram of surface state of [001] surface. Values 0 and π are Zak phases for lines normal to [001] surface. (c) [001] phonon surface states of Li_6WN_4 along $\bar{B} - \bar{B}_1$ and $\bar{B}_2 - \bar{B}_3$ surface paths;

knows that the nodal line along the Z-A path is topologically nontrivial, and should result in interesting surface states. As previously mentioned, owing to the S_{4z} symmetry, there are two nodal lines along the diagonal and clinodiagonal directions, respectively (see Fig. 2c). The shape of the nodal lines in the $k_z=\pi$ plane is shown in Fig. 3d, where one pair of nodal lines can be clearly observed (see the white lines). According to Fig. 2b, the nodal-line phonon is relatively flat in energy, and its energy variation is less than 0.3 THz (approximately 1.24 meV).

Remarkably, the ideal nodal-surface phonon and ideal nodal-line phonon constitute a hitherto unobserved type of bosonic excitation, namely, a nodal-lantern phonon, as illustrated in Fig. 2(c) and Fig. S1. Furthermore, as the existence of the two nodal surfaces and two nodal lines is guaranteed by symmetry, any 3D material with SG 137 must have nodal-lantern phonons as long as two of its phonon bands are separated from the others.

In the next step, the phonon surface states corresponding to the nodal-lantern phonon are studied. Because the two boundaries of the BZ (i.e., the $k_x = \pi$ and $k_y = \pi$ planes) are covered by the nodal surface, the [001] surface is the only surface that can experience a clear surface state. The corresponding surface BZ and some surface symmetry points ($\bar{A}, \bar{A}_1, \bar{A}_2, \bar{A}_3, \bar{B}, \bar{B}_1, \bar{B}_2, \bar{B}_3$) of the [001] surface are shown in Fig. 4a. The calculated

projected spectrum for the [001] surface along four surface paths $\bar{B} - \bar{B}_1$, $\bar{B}_1 - \bar{B}_2$, $\bar{B}_2 - \bar{B}_3$, and $\bar{B}_3 - \bar{B}$ are shown in Fig. 4c. Interestingly, evident [001] phonon surface states (highlighted by white arrows) can be found along the $\bar{B} - \bar{B}_1$ and $\bar{B}_2 - \bar{B}_3$ surface paths. However, the phonon surface states have disappeared along the $\bar{B}_1 - \bar{B}_2$ and $\bar{B}_3 - \bar{B}$ paths. We use the Zak phase to explain this peculiar surface state. Here, the relevant Zak phase is the Berry phase along a straight line parallel to the Γ -Z direction and across the bulk BZ:

$$Z(k_x, k_y) = \sum_{n \in occ} \oint_c A_z(\mathbf{k}) dk_z, \quad (3)$$

where A_z is the z-component of the Berry connection. The summation is performed for all the occupied bands. Owing to M_z symmetry, the Zak phase is quantized to 0 or π , which correspond to two topologically distinct phases. A π Zak phase generally indicates the existence of nontrivial topological surface state [53]. Because the two essential nodal lines along the Z-A path have nontrivial π Berry phases, their projections onto the [001] surface divides the surface BZ into four regions. Two regions have $Z=0$, and two regions have $Z=\pi$, as illustrated in Fig. 4b. Because each region occupies a quarter of the surface BZ, the topological surface state covers exactly half the surface BZ, which is consistent with the calculated results in Fig. 4c.

Before closing the article, we would like to present some important remarks about the topological signatures of the Li_6WN_4 phonon dispersion: (i) Although the existence of nodal surface states in the fermionic electronic structures of realistic materials has been predicted [27–29, 34], the proposed nodal surface states of phonons have not been studied by other researchers. This paper

presents the existence of ideal phononic nodal surface states in realistic materials *for the first time*. (ii) The predicted nodal surface is ideal in that it is nearly flat in energy with energy variations of less than 0.25 THz; in addition, the two relevant phonon bands are the only “clean” bands in the 22.5–24.5 THz range. (iii) The shape of the nodal structure in Li_6WN_4 (e.g., the nodal surface in the $k_x=\pi$ and $k_y=\pi$ planes and the nodal lines along the Z-A path) resembles that of a traditional lantern (see Fig. S1). We would like to point out that the nodal-lantern phonon is protected by symmetry and has never been reported before. These results can be used to investigate the entanglement between nodal-line and nodal-surface phonons.

In summary, based on first-principle calculations and symmetry analysis, a new topological phase was discovered: the nodal-lantern phonons in ternary nitride Li_6WN_4 are composed of two nodal-surface phonons in the $k_x=\pi$ and $k_y=\pi$ planes and one pair of nodal-line phonons in the $k_z=\pi$ plane. The existence of nodal-lantern phonons in Li_6WN_4 is protected by nonsymmorphic symmetries and time-reversal symmetry. Moreover, the phonon surface states in the [001] surface of this material were investigated; according to the results, the topological surface states of the nodal-lantern phonons cover exactly half the surface BZ. The presented results extend the concept of nodal surfaces to phonon systems, propose the existence of a undiscovered type of bosonic excitations, and predict the ideal material candidate.

Acknowledgments X.T. Wang is grateful for the support from the National Natural Science Foundation of China (No. 51801163) and the Natural Science Foundation of Chongqing (No. cstc2018jcyjA0765).

-
- [1] P. Wolfle, Reports on Progress in Physics, 81(3), 032501 (2018).
 - [2] N. Laflorencie, Physics Reports, 646, 1-59 (2016).
 - [3] Z. F. Wang, M. Y. Yao, W. Ming, L. Miao, F. Zhu, C. Liu, F. Liu, Nature Communications, 4(1), 1-6 (2013).
 - [4] A. A. Burkov, Nature Materials, 15(11), 1145-1148 (2016).
 - [5] C.-K. Chiu, J. C. Y. Teo, A. P. Schnyder, and S. Ryu, Reviews of Modern Physics, 88, 035005 (2016).
 - [6] H. Gao, J. W. Venderbos, Y. Kim, A. M. Rappe, Annual Review of Materials Research, 49, 153-183 (2019).
 - [7] N. Armitage, E. Mele, and A. Vishwanath, Reviews of Modern Physics, 90, 015001 (2018).
 - [8] S. S. Wang, Y. Liu, Z.-M. Yu, X. L. Sheng, S. A. Yang, Nature Communications, 8(1), 1-7 (2017).
 - [9] Y. Liu, Z.-M. Yu, C. Xiao, S. A. Yang, Physical Review Letters, 125, 076801 (2020).
 - [10] Y. Jin, R. Wang, H. Xu, Nano Letters, 18(12), 7755-7760 (2018).
 - [11] S.B. Zhang and J. Zhou, Physical Review B 101, 085202 (2020).
 - [12] Q. Xie, J. Li, S. Ullah, R. Li, L. Wang, D. Li, Y. Li, S. Yunoki, and X. Q. Chen, Physical Review B 99, 174306 (2019).
 - [13] Y. Liu, Y. Xu, S. C. Zhang, and W. Duan, Physical Review B 96, 064106 (2017).
 - [14] O. Stenull, C. L. Kane, T. C. Lubensky, Physical Review Letters, 117(6), 068001 (2016).
 - [15] N. P. Armitage, E. J. Mele, A. Vishwanath, Reviews of Modern Physics, 90(1), 015001 (2018).
 - [16] B. J. Yang, N. Nagaosa, Nature Communications, 5(1), 1-10 (2014).
 - [17] X. Wan, A. M. Turner, A. Vishwanath, and S. Y. Savrasov, Physical Review B 83, 205101 (2011).
 - [18] S. M. Young, C. L. Kane, Physical Review Letters, 115(12), 126803 (2015).
 - [19] A. A. Soluyanov, D. Gresch, Z. Wang, Q. Wu, M. Troyer, X. Dai, B. A. Bernevig, Nature, 527(7579), 495-498 (2015).
 - [20] B. Yan, C. Felser, Annual Review of Condensed Matter Physics, 8, 337-354 (2017).
 - [21] C. K. Barman, C. Mondal, B. Pathak, A. Alam, Physical

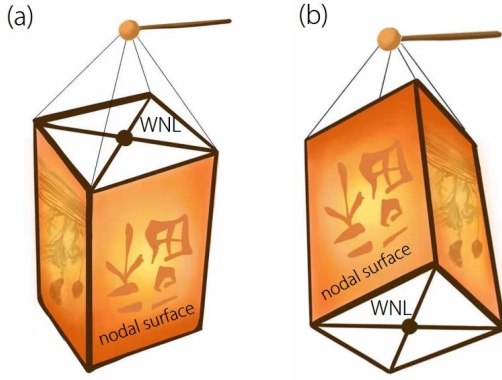


FIG. S1. (a) and (b) top and bottom views of lantern, which consists of a light with a transparent or translucent protective case.

- Review Materials, 4(8), 084201 (2020).
- [22] C. Fang, Y. Chen, H. Y. Kee, L. Fu, Physical Review B, 92(8), 081201 (2015).
 - [23] Y. Shao, A. N. Rudenko, J. Hu, Z. Sun, Y. Zhu, S. Moon, D. N. Basov, Nature Physics, 16(6), 636-641 (2020).
 - [24] D. S. Ma, J. Zhou, B. Fu, Z. M. Yu, C. C. Liu, Y. Yao, Physical Review B, 98(20), 201104 (2018).
 - [25] Z. Zhang, Z. M. Yu, S. A. Yang, Physical Review B, 103(11), 115112 (2021).
 - [26] C. Fang, H. Weng, X. Dai, Z. Fang, Chinese Physics B, 25(11), 117106 (2016).
 - [27] W. Wu, Y. Liu, S. Li, C. Zhong, Z. M. Yu, X. L. Sheng, S. A. Yang, Physical Review B, 97(11), 115125 (2018).
 - [28] C. Zhong, Y. Chen, Y. Xie, S. A. Yang, M. L. Cohen, and S. Zhang, Nanoscale 8, 7232 (2016).
 - [29] Q.-F. Liang, J. Zhou, R. Yu, Z. Wang, H. Weng, Physical Review B 93, 085427 (2016).
 - [30] T. Ojanen, Physical Review B, 87(24), 245112 (2013).
 - [31] Z.-M. Yu, W. Wu, X.-L. Sheng, Y. X. Zhao, S. A. Yang, Physical Review B 99, 121106(R) (2019).
 - [32] X. P. Li, B. Fu, D. S. Ma, C. Cui, Z. M. Yu, Y. Yao, arXiv preprint arXiv:2101.01523 (2021).
 - [33] S. S. Wang, W. K. Wu, S. Y. Yang, Acta Physica Sinica 68, 227101 (2019).
 - [34] Z. M. Yu, W. Wu, Y. Zhao, S. Yang, Physical Review B 93100, 041118 (2019).
 - [35] S. Singh, Q. S. Wu, C. Yue, A. H. Romero, A. A. Soluyanov, Physical Review Materials 2, 114204 (2018).
 - [36] J. Li, L. Wang, J. Liu, R. Li, Z. Zhang, X. Chen, Physical Review B, 101(8), 081403 (2020).
 - [37] J. Liu, W. Hou, E. Wang, S. Zhang, J. Sun, S. Meng, Physical Review B, 100(8), 081204 (2019).

- [38] T. Zhang, Z. Song, A. Alexandradinata, H. Weng, C. Fang, L. Lu, Z. Fang, Physical Review Letters 120, 016401 (2018).
- [39] H. Miao, T. T. Zhang, L. Wang, D. Meyers, A. H. Said, Y. L. Wang, Y. G. Shi, H. M. Weng, Z. Fang, M. P. M. Dean, Physical Review Letters 121, 035302 (2018).
- [40] Y. J. Jin, Z. J. Chen, B. W. Xia, Y. J. Zhao, R. Wang, H. Xu, Physical Review B 98, 220103(R) (2018).
- [41] J. Li, J. Liu, S. A. Baronett, M. Liu, L. Wang, R. Li, Y. Chen, D. Li, Q. Zhu, X. Chen, Nature Communications, 12, 1204 (2020).

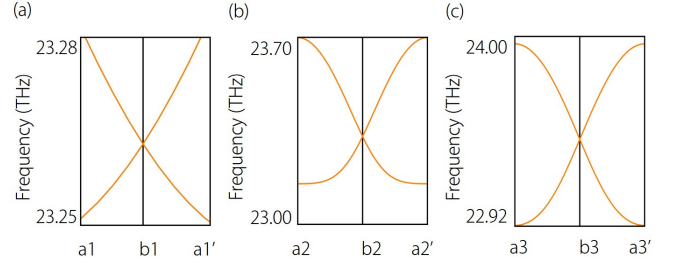


FIG. S2. (a)-(c) phonon dispersion along $a1-b1-a1'$, $a2-b2-a2'$, and $a3-b3-a3'$ paths, respectively.

- [42] B. Xia, R. Wang, Z. Chen, Y. Zhao, H. Xu, Physical Review Letters 123, 065501 (2019).
- [43] R. Wang, B. Xia, Z. Chen, B. Zheng, Y. Zhao, H. Xu, Physical Review Letters 124, 105303 (2020).
- [44] Q. Liu, H. Fu, G. Xu, R. Yu, R. J. Wu, The Journal of Physical Chemistry Letters 10, 4045 (2019).
- [45] J. Li, Q. Xie, J. Liu, R. Li, M. Liu, L. Wang, X. Q. Chen, Physical Review B, 101(2), 024301 (2020).
- [46] T. Zhang, H. Miao, Q. Wang, J. Lin, Y. Cao, G. Fabbris, A. Said, X. Liu, H. C. Lei, Z. Fang, H. M. Weng, and M. P. M. Dean, Physical Review Letters 123, 245302 (2019).
- [47] W. X. Yuan, J. W. Hu, Y. T. Song, W. J. Wang, Y. P. Xu, Powder diffraction, 20(1), 18-21 (2005).
- [48] E. K. Gross, R. M. Dreizler, (Eds.). (2013). Density functional theory (Vol. 337). Springer Science and Business Media.
- [49] J. P. Perdew, K. Burke, M. Ernzerhof, Physical Review Letters 80, 891 (1998).
- [50] A. Togo, I. Tanaka, Scripta Materialia 108, 1 (2015).
- [51] Q. Wu, S. Zhang, H. Song, M. Troyer, A. Soluyanov, Computer Physics Communications 224, 405 (2018).
- [52] Z. Yu, Z. Zhang, G. Liu, W. Wu, X. Li, R. Zhang, S. A. Yang, Y. Yao, arXiv preprint arXiv: 2102.01517 (2021).
- [53] Y.-H. Chan, C.-K. Chiu, M. Y. Chou, and A. P. Schnyder, Physical Review B, 93, 205132 (2016).